Application of Mathematical Absorber Reflection Suppression to Planar Near-Field Antenna Measurements

S.F. Gregson[#1], A.C. Newell[#2], G.E. Hindman[#3], M.J. Carey[#4]

[#]*Nearfield Systems Inc.*

19730 Magellan Drive, Torrance, CA 90502, USA

[1]*sgregson@nearfield.com*

[2]*anewell@nearfield.com*

[3]*ghindman@nearfield.com*

[4]*mcarey@nearfield.com*

***Abstract*— Nearly all antenna measurements are contaminated to some degree with fields scattered by objects within the environment of the test system. In many instances these reflections (*i.e.* multi-path) are found to constitute one of the most significant contributors to the facility-level error budget [1]. For some time, a frequency domain measurement and post-processing technique named Mathematical Absorber Reflection Suppression (MARS) has been successfully used to reduce range multi-path effects within spherical [2, 3, 4] and cylindrical near-field antenna measurement systems [5, 6]. More recently, a related technique has been developed for use with planar near-field antenna measurement systems [7]. This paper provides an introduction to the measurement technique and novel probe pattern corrected near-field to far-field transform algorithm. It then presents the most recent results of an on-going validation campaign which have been found to yield improvements comparable to those attained with the corresponding spherical and cylindrical MARS implementations. These results are discussed and conclusions presented.**

I. Introduction

Since its inception, the planar near-field (PNF) antenna measurement technique [8, 9] has developed into a powerful method for accurately and precisely characterising the performance of medium to high gain antennas at reduced range lengths. Due to the finite size of the planar sampling interval and thus the necessity to characterise primarily directional antennas, range multi-path effects have typically been considered to be of lesser importance in planar than in the corresponding cylindrical or spherical measurement techniques. Clearly, the directional nature of the higher gain antennas that are generally tested using planar systems results in the region of greatest field intensities being concentrated on the parts of the chamber situated immediately behind the scan plane and on the scanning robot itself. As a result of cost considerations, it has become widespread practice to concentrate the placement of absorbent material around the scanner itself; leaving, in some cases, much of the remainder of the chamber uncovered. Thus, in some circumstances multiple-reflections within the chamber can become significant, especially when measuring lower directive antennas exhibiting broader patterns, or low cross-polar patterns.

Typically, unwanted reflections are suppressed through the use of electromagnetic absorbing material, which tends to be costly, bulky, delicate, and can shed carbon dust. This absorber is usually shaped specifically so that its performance is optimised for use over a specific range of frequencies which necessarily render it less effective outside the designated frequency band. Whilst considerable effort is devoted to optimising the design and placement of this absorber, it is not possible to place the material everywhere, and some surfaces are inevitably left exposed, *e.g.* linear bearings of planar systems, lights, ventilation inlets, fire detection and suppression fittings, *etc.*. Clearly, any electromagnetic absorber which is used cannot be perfectly matched to fields incident at all directions, polarisations and frequencies. Thus in some cases, the resulting scattering can impede the measurements taken therein. Whilst considerable effort, ingenuity and resourcefulness have been devoted to quantifying and subsequently improving the quality of multi-path contaminated measurements taken in spherical near-field (SNF), far-field, compact antenna test ranges (CATR), and cylindrical near-field (CNF) facilities, planar near-field (PNF) systems have generally received far less attention in the open literature. Although hardware and software time-gating, aperture plane spatial filtering [7] and background subtraction techniques have all been proposed, the mode filtering methodologies that have proved so overwhelmingly successful when used with spherical and cylindrical systems have not previously been applied to the planar geometry.

II. Overview of Planar Mathematical Absorber Reflection Suppression

MARS is a sophisticated measurement and post-processing technique that has been developed to improve the quality of interferometric, *i.e.* phase coherent, antenna range measurements. The success of this technique has been attested to across a wide range of frequencies and on many different antenna types [5]. The general MARS principle involves a measurement and post-processing technique that

analyses the measured data before utilising a special filtering process to suppress undesirable scattered fields. This frequency-domain technique is completely general requiring only a minimum amount of information about the antenna under test (AUT) and measurement configuration. Whilst techniques for suppressing range reflections in planar near-field systems are not new, [10, 11], uniquely the planar MARS (P-MARS) technique requires no additional hardware, and introduces no additional a priori assumptions regarding the structure, arrangement, or distribution of the current sources. Thus, this technique is equally applicable to aperture and non-aperture type antennas and it is only assumed that the current sources occupy a finite region of space, and that the various scatterers within the chamber are outside of this region of space.

A. Planar MARS Measurement Configuration

All forms of MARS processing require the AUT to be offset from the origin of the measurement co-ordinate system by a distance at least equal to its largest dimension [7, 5]. This displacement is illustrated schematically in Fig. 1 for the SNF case. By way of a comparison, Fig. 2 shows the same AUT located conventionally at the origin of the spherical measurement co-ordinate system. The conceptual minimum spheres are also shown for each of these cases which are centred about the intersection of the orthogonal θ- and ϕ-axes (shown in red). For cylindrical MARS, the displacement is also measured from the axis of rotation.

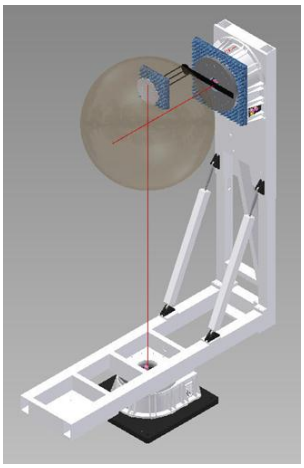

Fig. 1 AUT measured with offset from rotation origin with larger MRE shown.

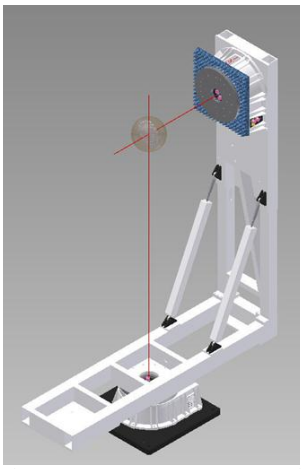

Fig. 2 AUT measured conventionally at rotation origin with smaller MRE shown.

Uniquely, for the planar case the displacement is measured from the centre of the aperture of the near-field probe when located at the centre of the scan plane. This difference is illustrated in Fig. 3 where a combination planar, cylindrical, spherical (PCS) system can be seen. Here, the AUT displacement for the spherical and cylindrical cases can be seen depicted by the red arrows, whilst the corresponding displacement for the planar case is shown with the blue arrows. This subtle difference follows from noting that mathematically, a displacement from origin of measurement co-ordinate system in a spherical (or cylindrical) near-field antenna measurement is indistinguishable from the AUT-to-probe separation in a planar near-field antenna measurement. Indeed, these displacements are the same as those used when reconstructing the aperture illumination function of an AUT when using microwave holographic metrology (MHM). Conventionally, planar near-field measurements are made with an antenna-to-probe distance of two or more wavelengths. This has become common practice as the lower limit is imposed by the requirement to take data only outside of the reactive near-field whilst simultaneously minimising the size of the planar sampling interval.

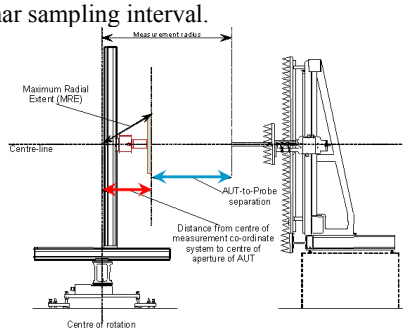

Fig. 3 Extension of MARS to the planar geometry. S-MARS and C-MARS displacement depicted in red, with P-MARS displacement depicted in blue.

Thus, in order for the P-MARS multipath-suppression technique to be capable of identifying and effectively suppressing range multi-path interference, the AUT-to-probe separation must be increased from the order of a few wavelengths to a distance that is at least equal to the physical size of the AUT. Thus, like the spherical and cylindrical analogues, P-MARS necessitates the acquisition of additional near-field data as the measurement area must be increased. However, unlike SNF or CNF measurements, P-MARS does *not* require a reduction in the sampling increment and conventional half-wavelength sample spacing is adequate.

B. Planar MARS Processing and Transformation Algorithm

A complete and detailed description of the P-MARS transformation and post-processing algorithm is beyond the scope of this paper. However, an overview of the novel processing is presented with this section with a more detailed mathematical treatment being left to the open literature [5, 7, 9]. Fig. 4 contains a false-colour checkerboard plot of the measured *x*-polarised near-electric-field of an *x*-band standard gain horn (SGH) that was acquired using an NSI-300V-12x12 12' by 12' (3.6 x 3.6 m) vertical planar near-field test system. The corresponding probe pattern corrected far electric field can be seen presented in Fig. 5 having been tabulated on a regular azimuth over elevation plotting co-ordinate system and resolved onto a Ludwig II polarisation basis and represents the far-field data as obtained using standard planar processing [8, 9]. Here, the effects of range multipath can be seen as ripple on the antenna pattern and as wide out high angular frequency noise. Although not shown here (only the magnitude of the field is plotted) the far electric field of the AUT has been mathematically translated to the origin of the measurement co-ordinate system through the application of a simple parabolic phase change [7, 9].

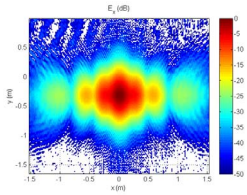

Fig. 4 Planar near-field antenna measurement of AUT.

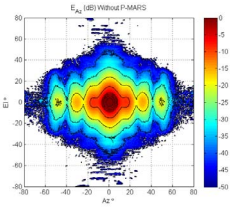

Fig. 5 Multipath contaminated probe corrected far-field pattern of AUT.

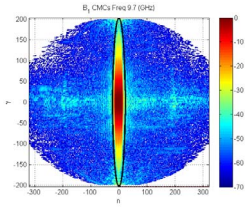

Fig. 6 *x*-axis CMCs of AUT having been mathematically translated back to origin of measurement system.

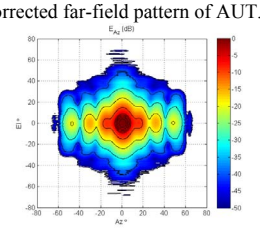

Fig. 7 Far-field pattern of AUT after spurious higher order modes have been filtered out.

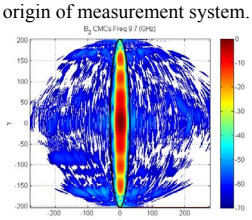

Fig. 8 *y*-axis CMCs of AUT.

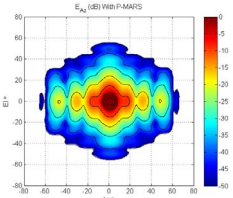

Fig. 9 Far-field pattern of AUT with P-MARS processing applied.

In principle, it is possible to obtain spherical mode coefficients (SMC) or cylindrical mode coefficients (CMC) from the plane wave spectrum (PWS) by using the field equivalence principle and field matching outside the excluded region. However, due to their greater numerical stability and the enormous ease and efficiency with which they can be obtained from far electric fields, in this instance it was preferable to work with CMCs. Here, an azimuth over elevation co-ordinate system was chosen specifically as the equivalent CMCs can be obtained directly from this data through the evaluation of a series of one-dimensional inverse Fourier transforms [5, 7],

$$B_n^1(\gamma) = -\frac{(-j)^{-n}}{4\pi\kappa}\int_0^{2\pi} E_A(r\to\infty, A, E)e^{-jnA}dA \qquad (1)$$

$$B_n^2(\gamma) = j\frac{(-j)^{-n}}{4\pi\kappa}\int_0^{2\pi} E_E(r\to\infty, A, E)e^{-jnA}dA \qquad (2)$$

Thus, it is possible to obtain CMCs from a planar-near field measurement rigorously without recourse to approximation. CMCs are complex numbers that are functions of the polarization index *s*, the ϕ index *n* and the Fourier variable γ. Fig. 6 contains a false colour checkerboard plot of the magnitude of the CMCs modes for $s = 1$, *i.e.* B^1 as a function of *n* and γ (horizontal axis is *n*, and vertical axis is γ) and which correspond to the multipath contaminated far-field pattern of the SGH that are shown in Fig. 5. For the cases of spherical and cylindrical near-field measurements the highest order mode index is related to the maximum radial extent (MRE), denoted with r_{t0}, of the equivalent measurement. Here, the conceptual MRE corresponds to half the width of the AUT. Thus, from standard cylindrical theory, it is possible to filter out all higher order modes without affecting the integrity of the underlying antenna pattern function. When expressed mathematically the band-pass mode filter function can be expressed as,

$$B_n^s(\gamma)\Big|_{s=1,2} = \begin{cases} B_n^s(\gamma) & n^2 + (\gamma r_{t0})^2 \le (k_0 r_{t0})^2 \\ 0 & \text{elsewhere} \end{cases} \qquad (3)$$

It is clear that the CMCs associated with the AUT are confined to a narrow band that are tightly distributed about $n = 0$, *i.e.* in the centre of the plot with $|n| < 30$. As the total power radiated by the AUT must be conserved, the amount of power per mode must increase as the total number of modes associated with the AUT decreases. As the amount of noise per mode can be seen to be roughly constant, in this case at circa -60 dB with respect to the maximum level, the effective system signal to noise (SNR) ratio of the measurement is significantly increased. Crucially, and as has been observed previously with S- and C-MARS, although the AUT has been translated back to the origin of the measurement co-ordinate system, this is not the case for the scatterers which are spatially extended and are represented by many higher order modes. In effect, the contributions in the CMC domain of the AUT and the scatterers are separated so that they do not interfere and are in essence orthogonalised from one another. The mode filtered far-field pattern can be obtained by evaluating the inverse of equations 1 and 2 namely [5, 7],

$$E_A(r\to\infty, A, E) = -2k_0\cos E\sum_{n=-\infty}^{\infty}(-j)^n B_n^1(\gamma)e^{jnA} \qquad (4)$$

$$E_E(r\to\infty, A, E) = -2jk_0\cos E\sum_{n=-\infty}^{\infty}(-j)^n B_n^2(\gamma)e^{jnA} \qquad (5)$$

Fig. 7 presents the mode filtered far-field pattern. This mode filtering technique has clearly suppressed the effects of scattering although this is principally limited to contributions in the *xz*-plane. However, scattering artefacts that have a component in the *yz*-plane, are less effectively suppressed by this processing. Fortunately, it is a trivial matter to repeat this modal filtering once the partially filtered antenna pattern function has been rotated by 90° about the positive *z*-axis. Thus, Fig. 8 contains the equivalent false colour checkerboard plot of the magnitude of the CMCs computed for the *y*-axis. Here, as expected, the background noise level is lower than was previously the case with many modes being more than 70 dB below the peak. As before, these modes can be filtered to remove higher order modes that are associated with scattering in the second axis. Here however, the band-pass mode filter function will depend upon the orthogonal dimension of the antenna. Thus, by implementing this processing sequentially in both horizontal and vertical axes, *all* of the range scattering effects can be very effectively suppressed. The final P-MARS processed pattern can be found presented in Fig. 9.

III. MEASURED RESULTS

Experimental verification of the P-MARS measurement technique was primarily based upon assessing the repeatability between successive measurements where a single parametric change had been introduced. The intent being that the P-MARS processing should be capable of compensating

for the change. Fig. 10 shows a NSI-300V-12x12, 12'×12' planar near-field system installed within a partially absorber lined chamber. This system was used to acquire an NSI-RF-SG90 *x*-band SGH which was used as an AUT during the validation campaign described in the following sections.

A. Additional Scatterer Suppression

The first measurements consisted of taking an initial baseline acquisition after which a large aluminium scatterer was placed in the region of greatest field intensity on the rear wall immediately behind the centre of the scan plane. This arrangement can be seen presented in Fig. 11. This was intended to introduce a large, worst-case, specular reflection into the measured antenna radiation pattern so that the effects of the P-MARS processing could be clearly observed and easily verified.

Fig. 10 NSI-300V-12x12 system installed within a partially absorber lined chamber.

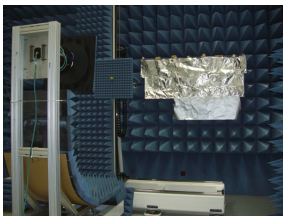

Fig. 11 NSI-300V-12x12 system shown with reflector placed behind scan plane.

Fig. 5 contains a false colour plot of the baseline SGH measurement. Here, some low level scatter can be seen at wide polar angles which manifest themselves as high frequency ripple (speckle) at approximately the -30 dB level. Fig. 12 contains the far-field pattern of the scattering contaminated SGH measurement as obtained using conventional planar processing. Conversely, Fig. 13 contains an equivalent plot of the same measured data after P-MARS processing has been applied.

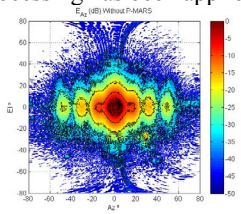

Fig. 12 Measurement with reflector on back wall.

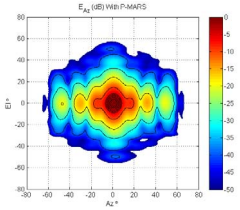

Fig. 13 Measurement with reflector and P-MARS processing.

The high frequency ripple has been effectively eradicated together with the spurious large amplitude scattering that is clearly evident on the unfiltered results at $Az = 25°$, $El = -25°$. Fig. 14 contains azimuth cardinal cuts of the reference measurement and multipath contaminated measurement plotted together with the equivalent multipath level (EMPL) [9]. This can be thought of as representing the amplitude necessary to make the different pattern functions equal. Fig. 15 contains an equivalent plot after P-MARS processing has been applied. Here, it can be seen that the EMPL has decreased by circa 20 dB which is expected as the agreement between the respective plots is very encouraging. The poorest agreement is shown by the EMPL to be for azimuth angles at *circa* 20° which correspond to the region where the scatterer had the greatest effect. However, the level is circa -50 dB which is very encouraging as it represents a 10 dB improvement over the reference measurement and is 40 dB below the antenna pattern.

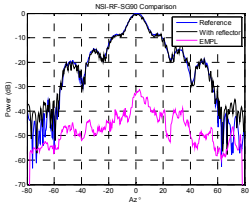

Fig. 14 Reference measurement versus measurement with reflector.

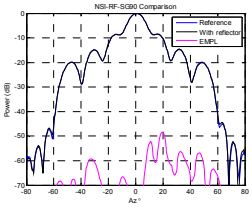

Fig. 15 P-MARS processed reference measurement and reflector measurement.

B. Secondary Source Suppression

Numerous tests were conducted with reflecting material placed at various locations within the test environment. However, even for the worst case example, presented in Section A, the magnitude of the specular reflections were found to be comparatively small, *e.g.* 20 dB beneath the peak of the antenna pattern. Thus, in an attempt to create a more significant disturbance, a secondary higher gain source antenna was introduced into the measurement and used to synthesize a large amplitude scatterer in a known and controllable manner. This configuration can be seen presented in Fig. 16 and 17 where the separation between the AUT and secondary source was varied (marked with a circle).

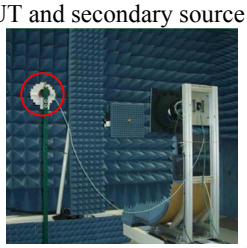

Fig. 16 Secondary sources with a large AUT-to-source separation.

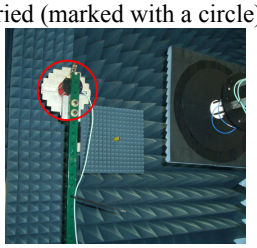

Fig. 17 Secondary source with a smaller AUT-to-source separation.

As before, baseline measurements were taken in the absence of the secondary source. These measurements were then repeated with the secondary source radiating at a series of displacements in the *x*-axis. These measurements were transformed to the far-field with P-MARS processing having been applied to compensate for the deleterious effects of the secondary source. Fig. 18 contains a false-colour plot of the amplitudes of the CMC's modes for $s = 1$ resulting from a scan taken with the centre of the secondary source located 15.5" away from the centre of the AUT with the source boresight pointing perpendicular to the scan-plane, and emitting half of the power of the AUT. Here, the CMC are widely distributed across the mode domain with no clear delineation between those modes that are associated with the AUT and those modes associated with the secondary source. Conversely, Fig. 19 shows a similar plot only here the AUT has been mathematically translated back to the origin of the measurement co-ordinate system and clearly shows the separation of AUT and secondary source CMCs. As expected, inspection of Fig. 19 reveals that those modes associated with the AUT are tightly distributed and centred about mode index

n = 0 and are separated from those modes that are associated with the secondary source which are now centred about the higher order n = 80 mode index. As before the black ellipse denotes the highest order CMC that can be produced by the AUT. As the majority of the modes that are associated with the secondary source lie outside of this domain, then they can be filtered out without altering the underlying antenna pattern.

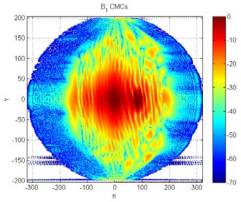

Fig. 18 CMCs Calculated from planar measurement.

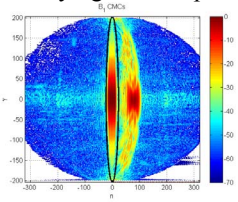

Fig. 19 CMCs after AUT translated to origin.

Respectively, Fig. 20 and 21 contain the far-field patterns of the SGH before and after P-MARS processing has been applied. These results are particularly encouraging as they show an almost complete suppression of the additional energy which was caused by the introduction of the secondary source with the spurious high frequency ripple that is present in the unfiltered results being clearly absent from the processed equivalent plot.

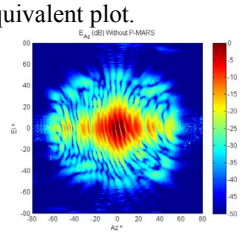

Fig. 20 Measurement of SGH with secondary source radiating.

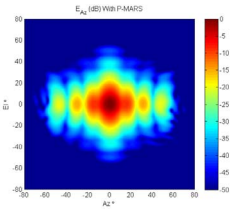

Fig. 21 SGH measurement with secondary source radiating and P-MARS processing applied.

This effect is further illustrated by comparing the azimuth cardinal cut without P-MARS processing, shown in Fig. 22, with the P-MARS processed equivalent, shown in Fig. 23. Here it is clear that the difference level which is characterised by the EMPL had decreased to below -60 dB over the majority of the far-field pattern.

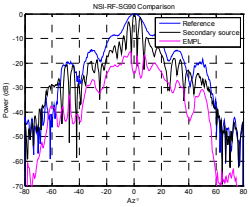

Fig. 22 Reference measurement versus measurement with secondary source.

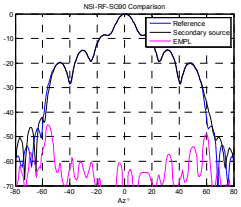

Fig. 23 Reference measurement versus measurement with secondary source with P-MARS processing.

Thus, and as required, P-MARS will attenuate spurious modes irrespective of whether they are a result of an; unwanted secondary source, or a spurious reflection from imperfections in the anechoic test chamber. Crucially, the results were comparable even when the secondary source was located as close as one wavelength away from the AUT. Thus for the fist time, P-MARS processing has been demonstrated to be equally effective at suppressing large field intensities.

IV. Summary and Conclusions

Planar MARS processing can be used with a very high degree of confidence since all the steps in the measurement and analysis are consistent with the well-established principles of standard near-field theory and measurement technique, and all comparisons thus far have proved overwhelmingly positive. The offset of the AUT and the resulting larger sampling interval are estimated using conventional rules, and the mathematical translation of the AUT to the origin is rigorous. The selection of the mode cut-off for the translated pattern is based on the physical dimensions of the AUT and its translated location. The final result with MARS processing can be degraded if the sampling area of the near-field data is too restrictive, or the mode filter is too tight, *i.e.* abrupt, but importantly these parameters are controlled by the user. The results of planar MARS processing will reduce but cannot entirely eliminate the effect of scattering. As has been demonstrated, this novel frequency domain measurement and processing technique is entirely general and can be used to achieve acceptable results with use of minimal absorber or even without the use of an anechoic chamber, even when testing lower gain antennas. MARS has been found to improve the reflection levels in traditional anechoic chambers allowing improved accuracy as well as offering the ability to use existing chambers down to lower frequencies than the absorber might otherwise suggest.

References

[1] A.C. Newell, "Error Analysis Techniques for Planar Near-field Measurements", IEEE Transactions on Antennas and Propagation, vol. AP-36, pp. 754-768, June 1988.

[2] G.E. Hindman, A.C. Newell, "Reflection Suppression in a large spherical near-field range", AMTA 27th Annual Meeting & Symposium, Newport, RI, October. 2005.

[3] G.E. Hindman, A.C. Newell, "Reflection Suppression To Improve Anechoic Chamber Performance", AMTA Europe 2006, Munich, Germany, March 2006.

[4] G.E. Hindman, A.C. Newell, "Mission To MARS - In Search of Antenna Pattern Craters", AMTA 28th Annual Meeting & Symposium, St. Louis, MO, November 2007.

[5] S.F. Gregson, A.C. Newell, G.E. Hindman, "Reflection Suppression In Cylindrical Near-Field Antenna Measurement Systems - Cylindrical MARS", AMTA 31st Annual Meeting & Symposium, Salt Lake City, UT, November 2009.

[6] S.F. Gregson, A.C. Newell, G.E. Hindman, M.J. Carey, "Comparison of Cylindrical and Spherical Mathematical Absorber Reflection Suppression", Loughborough Antenna And Propagation Conference, November 2010.

[7] S.F. Gregson, A.C. Newell, G.E. Hindman, M.J. Carey, "Extension of The Mathematical Absorber Reflection Suppression Technique To The Planar Near-Field Geometry", AMTA, Atlanta, October 2010.

[8] D.M. Kerns, "Plane-Wave Scattering-Matrix Theory Of Antennas And Antenna-Antenna Interactions", Nat. Bur. Stand. (U.S.) Monograph 162, June 1981.

[9] S.F. Gregson, J. McCormick, C.G. Parini, "Principles of Planar Near-Field Antenna Measurements", The Institution of Engineering and Technology, UK, 2007.

[10] G.E. Hindman, D. Slater, "Error Suppression Techniques for Near-Field Antenna Measurements", AMTA Meeting and Symposium, October, 1989.

[11] J. van Norel, A.H. van Gastel, V.J. Vokurka, J. Neve, J.F. Coroller, "Application of Flexible Scanning in Advanced APC-Techniques", AMTA 16th Annual Meeting & Symposium, October, 1994.